
Article:
Reed, Christopher Paul, Evans, Mathew John orcid.org/0000-0003-4775-032X, Di Carlo, P. et al. (2 more authors) (2015) Interferences in photolytic NO2 measurements : explanation for an apparent missing oxidant? Atmospheric Chemistry and Physics Discussions. pp. 28699-28747. ISSN 1680-7367

https://doi.org/10.5194/acpd-15-28699-2015

Atmos. Chem. Phys. Discuss., 15, 28699–28747, 2015
www.atmos-chem-phys-discuss.net/15/28699/2015/
doi:10.5194/acpd-15-28699-2015

Atmospheric Chemistry and Physics Discussions

Interferences in photolytic NO_2 measurements: explanation for an apparent missing oxidant?

C. Reed[1], M. J. Evans[1,2], P. Di Carlo[3,4], J. D. Lee[1,2], and L. J. Carpenter[1]

[1]Wolfson Atmospheric Chemistry Laboratories, Department of Chemistry, University of York, Heslington, York, YO10 5DD, UK
[2]NCAS, School of Earth and Environment, University of Leeds, Leeds, LS2 9JT, UK
[3]Centre of Excellence CEMTEPs, Universita' degli studi di L'Aquila, Via Vetoio, 67010 Coppito, L'Aquila, Italy
[4]Dipartmento di Scienze Fisiche e Chimiche, Universita' degli studi di L'Aquila, Via Vetoio, 67010 Coppito, L'Aquila, Italy

Received: 6 October 2015 – Accepted: 7 October 2015 – Published: 23 October 2015

Correspondence to: J. D. Lee (james.lee@york.ac.uk)

Published by Copernicus Publications on behalf of the European Geosciences Union.

Abstract

Measurement of NO_2 at low concentrations is non-trivial. A variety of techniques exist, with the conversion of NO_2 into NO followed by chemiluminescent detection of NO being prevalent. Historically this conversion has used a catalytic approach (Molybdenum); however this has been plagued with interferences. More recently, photolytic conversion based on UV-LED irradiation of a reaction cell has been used. Although this appears to be robust there have been a range of observations in low NO_x environments which have measured higher NO_2 concentrations than might be expected from steady state analysis of simultaneously measured NO, O_3, JNO_2 etc. A range of explanations exist in the literature most of which focus on an unknown and unmeasured "compound *X*" that is able to convert NO to NO_2 selectively. Here we explore in the laboratory the interference on the photolytic NO_2 measurements from the thermal decomposition of peroxyacetyl nitrate (PAN) within the photolysis cell. We find that approximately 5 % of the PAN decomposes within the instrument providing a potentially significant interference. We parameterize the decomposition in terms of the temperature of the light source, the ambient temperature and a mixing timescale (~ 0.4 s for our instrument) and expand the parametric analysis to other atmospheric compounds that decompose readily to NO_2 (HO_2NO_2, N_2O_5, $CH_3O_2NO_2$, $IONO_2$, $BrONO_2$, Higher PANs). We apply these parameters to the output of a global atmospheric model (GEOS-Chem) to investigate the global impact of this interference on (1) the NO_2 measurements and (2) the NO_2 : NO ratio i.e. the Leighton relationship. We find that there are significant interferences in cold regions with low NO_x concentrations such as Antarctic, the remote Southern Hemisphere and the upper troposphere. Although this interference is likely instrument specific, it appears that the thermal decomposition of NO_2 within the instrument's photolysis cell may give an explanation for the anomalously high NO_2 that has been reported in remote regions, and would reconcile measured and modelled NO_2 to NO ratios without having to invoke novel chemistry. Better instrument characterization, coupled to instrumental designs which reduce the heating within the cell seem likely

ACPD
15, 28699–28747, 2015

to minimize the interference in the future, thus simplifying interpretation of data from remote locations.

1 Introduction

Accurate quantification of atmospheric nitrogen oxide (NO_x which is predominantly NO + NO_2 but includes small contributions from NO_3, N_2O_5, HONO, HO_2NO_2 etc.) concentrations is crucial for many aspects of tropospheric chemistry. NO_x plays a central role in the chemistry of the troposphere, mainly through its impact on ozone (O_3) and hydroxyl (OH) radical concentrations. O_3 is a climate gas (Wang et al., 1995), adversely impacts human health (Mauzerall et al., 2005; Skalska et al., 2010) and leads to ecosystem damage (Ainsworth et al., 2012; Ashmore, 2005; Hollaway et al., 2012). It is produced through the reaction of peroxy radicals (HO_2 and RO_2) with NO (Dalsøren and Isaksen, 2006; Lelieveld et al., 2004). The OH radical is the primary oxidizing agent in the atmosphere (Crutzen, 1979; Levy II, 1972) as it controls the concentration of other key atmospheric constituents such as methane (CH_4), carbon monoxide (CO) and volatile organic compounds (VOCs). It is both produced through the reaction of NO with HO_2 and is lost by its reaction with NO_2. NO_2 itself poses a public health risk (Stieb et al., 2002). Thus understanding the sources, sinks and distribution of NO_x is of central importance to understanding the composition of the troposphere.

During the daytime there is fast cycling between NO and NO_2, due to the rapid photolysis of NO_2 and the reaction NO and O_3 to form NO_2 (Kley et al., 1981).

$$NO_2 + h\nu(< 410\,\text{nm}) \rightarrow NO + O(^3P) \quad \text{(R1)}$$

$$O_2 + O(^3P) + M \rightarrow O_3 + M \quad \text{(R2)}$$

$$O_3 + NO \rightarrow O_2 + NO_2 \quad \text{(R3)}$$

ACPD
15, 28699–28747, 2015

Placing NO_2 into steady state and assuming that these three reactions are the only chemistry occurring leads to the Leighton relationship, ϕ (Leighton, 1961), in Eq. (1).

$$1 = \frac{k_1 [NO] [O_3]}{j_{NO_2} [NO_2]} = \phi \quad (1)$$

The quantities in the relationship are readily measured and deviations from unity have been interpreted to signify missing (i.e. non ozone) oxidants of NO. These perturbations have been used to infer the existence of oxidants such as peroxy radicals, or halogen oxides in the atmosphere (Bauguitte et al., 2012; Cantrell et al., 2003; Frey et al., 2015).

The concentration of NO_x varies from > 100 ppb (parts per billion) next to roads (Carslaw, 2005; Pandey et al., 2008) to low ppt (parts per trillion) in the remote atmosphere (Lee et al., 2009). Direct transport of NO_x from polluted to remote regions is not efficient, because NO_x is removed from the atmosphere on a timescale of around a day by the reaction of NO_2 with OH and the hydrolysis of N_2O_5 on aerosol surfaces (Brown et al., 2004; Dentener and Crutzen, 1993; Riemer et al., 2003). Instead, reservoir species such as peroxy-acetyl nitrate are made in polluted regions (which are high in both NO_x and peroxy-acetyl precursors such as acetaldehyde) and are subsequently transported to remote regions where they thermally breakdown to release the NO_x.

$$CH_3CHO + OH^\bullet + O_2 \rightarrow CH_3C(O)OO^\bullet + H_2O \quad (R4)$$

$$CH_3C(O)OO^\bullet + NO_2 + M \rightleftarrows CH_3C(O)O_2NO_2 + M \quad (R5)$$

The equilibrium between peroxy-acetyl radicals, NO_2 and PAN (Reactions R4 and R5) is highly temperature sensitive. Thus the PAN lifetime changes from 30 min at 25 °C (Bridier et al., 1991) to 5.36 years at −26 °C (Kleindienst, 1994).

Measurements of NO_x species in the remote atmosphere have been made over the last 40 years. Multiple in-situ techniques are available such as LIF (Matsumoto and Kajii, 2003), Cavity Ring Down (Osthoff et al., 2006), and QCL – Quantum Cascade Laser (Tuzson et al., 2013). However, probably the most extensively used approach has been based on the chemiluminescent reaction between NO and O_3. This exploits

ACPD
15, 28699–28747, 2015

the reaction between NO and O_3 (Reaction R6) which generates a vibrationally excited NO_2 molecule which decays into its ground state through the release of a photon (Reaction R7) (Clyne et al., 1964).

$$NO + O_3 \rightarrow NO_2^* \quad \text{(R6)}$$

$$NO_2^* \rightarrow NO_2 + h\nu \quad (> 600\,\text{nm}) \quad \text{(R7)}$$

This forms the basis of the chemiluminescence analysis of NO (Drummond et al., 1985; Fontijn et al., 1970; Kelly et al., 1980; Peterson and Honrath, 1999). The number of photons emitted by the decay of excited NO_2^* to NO_2 is proportional to the NO present before reaction with O_3 (Drummond et al., 1985). The photons emitted are detected by a cooled photomultiplier tube (PMT) with the sample under low pressure (to maximize the fluorescence lifetime of the NO_2^*), to yield a signal which is linearly proportional to the number density of NO in the sample gas (Fontijn et al., 1970).

With NO chemiluminescence analysers it is also possible to analyse NO_2 if it is first converted to NO, either catalytically (typically heated Molybdenum) as in Reaction (R8) (Villena et al., 2012), or by converting NO_2 into NO photolytically (Ryerson et al., 2000), exploiting Reaction (R1).

$$Mo + 3NO_2 \rightarrow MoO_3 + 3NO \quad \text{(R8)}$$

To measure NO and NO_2, the sample flows through the NO_2 to NO converter (of either type) to the reaction chamber where the $NO + O_3$ reaction occurs and the decay of NO_2^* to NO_2 allows the concentration of $NO + NO_2$ in the air to be measured. Then, the sample flow is switched to bypass the NO_2 to NO converter. Now, only NO present in the sample is detected in the chemiluminescence reaction. The NO signal is then subtracted from the $NO + NO_2$ (NO_x) signal giving the NO_2 signal.

Measurements of NO and NO_2 have been successfully made in a range locations using the chemiluminescence technique (Huntrieser et al., 2007; Lee et al., 2009; Peterson and Honrath, 1999; Zhang et al., 2008). However, measurements made in remote (low NO_x) locations, such as Antarctica and in the open ocean have at times

ACPD
15, 28699–28747, 2015

identified an unexplained imbalance in the Leighton relationship (Cantrell et al., 1997; Hosaynali Beygi et al., 2011). Measured NO_2 concentrations are higher than would be expected from the observed NO, O_3, JNO_2 along with reasonable concentrations of other oxidants (peroxy radicals, halogen oxides). Various explanations have been posited in order to overcome the apparent oxidation gap, typically relying on a mystery unmeasured oxidant, or pushing known chemistry into theoretical realms by theorizing high turnover of short-lived species which may only have been measured in trace quantities (Cantrell et al., 2003; Frey et al., 2013, 2015; Hosaynali Beygi et al., 2011). An alternative explanation would be an unknown interference on the NO_2 measurement increasing its apparent concentration.

Here we explore the potential of PAN to interfere with chemiluminescence NO_2 measurements. In Sect. 2 we provide some details of the experimental studies undertaken. In Sect. 3 we describe the results of experiments introducing differing concentrations of PAN into NO_2 converter/chemiluminescence systems. In Sect. 4 we analyse the potential for errors with different NO_x systems to investigate the interference on the measurement of NO_2 from PAN. In Sect. 5 we evaluate the impact of this interference on NO_2 measurements and on the Leighton relationship through the use of a global model and provide conclusions in Sect. 6.

2 Experimental details

In Sect. 2.1 we describe the two chemiluminescence instruments used for the analysis. The NO_2 converters are described in Sect. 2.2. In Sect. 2.3 and the LIF instrument used to provide a reference analysis is described. We describe our protocol for production of PAN by acetone photolysis in Sect. 2.4. We provide details of the zero air generation in Sect. 2.5. Then in Sect. 2.6 we describe the experimental methodology of PAN interference tests and residence time tests in Sect. 2.7.

ACPD
15, 28699–28747, 2015

2.1 Instrumentation

Chemiluminescent measurements were performed using dual channel Air Quality Design Inc. (Golden, Colorado, USA) instruments equipped with UV-LED based photolytic NO_2 converters – commonly referred to as Blue Light Converters (BLCs). Two similar instruments were employed; the "laboratory" NO_x analyser (Sect. 2.1.1) – on which the majority of the experiments were performed and the "aircraft" NO_x analyser (Sect. 2.1.2) on which only temperature controlled BLC experiments were performed.

Both instruments feature independent mass flow controlled sample flows on each channel (NO and NO_x). The wetted surfaces of the instrument are constructed of 1/4 inch PFA tubing, with the exception of 316 stainless steel unions/MFC internals.

Both instruments are calibrated for NO by internal, automatic standard addition. Calibration for NO_2 converter efficiency is by internal automatic gas phase titration of NO with O_3 to form NO_2 with the NO signal measured with the BLC lamps active and inactive as described by (Lee et al., 2009). Artefacts in both NO and NO_2 are measured whilst sampling zero air.

2.1.1 Laboratory NO_x analyser

The laboratory NO_x analyser from Air Quality Design, Inc. (AQD) is a custom dual channel instrument designed for fast response and very low limit of detection (LOD). The dual channel design means that there are effectively two separate NO chemiluminescence instruments working in parallel. Both channels have identical flow paths and share identical duplicate equipment; ozonizers, MFCs, PMTs etc. Both channels share the same vacuum pump – an Edwards XDS 35i. One channel is equipped with a BLC immediately in front of the MFC flow control/low pressure side of the system. It is possible to analyse NO with one channel, and NO_x with the other to provide a constant, fast measurement (1 Hz) of NO and NO_2. Alternatively, a single channel can be used with the BLC in a switching mode so that it is active for only 40 % of the duty cycle to provide NO and NO_2 measurement – the other 60 % of the duty cycle is devoted to NO (40 %)

ACPD
15, 28699–28747, 2015

and to measuring zero (20 %). In this case the second channel might be used for NO_y by connection of a catalytic converter to the inlet as is the set-up at the Cape Verde Atmospheric Observatory GAW station (Lee et al., 2009). In these experiments both modes were used in order to replicate different instrument designs; a switching mode with 40 % duty cycle of the NO_2 converter and a total sample flow of 1 standard L min^{-1}, and a parallel mode with 100 % duty cycle of the NO_2 converter with a total sample flow of 2 standard L min^{-1}.

The nominal sensitivity of the instrument is 3.5 and 4.0 cps ppt^{-1} on channel 1 (NO) and channel 2 (NO and NO_x) respectively. The 1 min LOD is ~ 2.5 pptv.

2.1.2 Aircraft NO_x analyser

The aircraft NO_x analyser, also from AQD, operates similarly to the lab NO_x analyser with some alterations to make it suited to aircraft operation but which do not affect its use on the ground. It can therefore be considered analogous to the lab NO_x analyser with the exception of the BLC which is of a non-standard design in that it uses six more powerful UV-diodes which require active Peltier/forced air-cooling controlled by a PID in order to maintain an operating temperature close to ambient. The special requirements for this NO_2 converter are primarily because of the high sample flow rates needed to measure NO_x fluxes on an airborne platform at reduced pressure. However, in this study the sample flow rate was a constant 1 standard L min^{-1} per channel at ambient temperature and pressure.

The nominal sensitivity of the instrument is 8.3 and 11.6 cps ppt^{-1} on channel 1 (NO) and channel 2 (NO_x) respectively. The 1 min LOD is ~ 1.0 pptv.

2.2 NO_2 converters

Photolytic converters for the two chemiluminescent systems were supplied by Air Quality Design and manufactured according to their proprietary standards (Buhr, 2004, 2007). Systems have also been developed subsequently (Pollack et al., 2011;

ACPD
15, 28699–28747, 2015

Sadanaga et al., 2010) with variations implementation, though similar operation and results. Experiments with either NO_2 converter were carried out at ambient temperature and pressure; 20 °C, 1 atm.

Photolytic converters employ Reaction (R1) to convert NO_2 to NO over a narrow wavelength band, thus providing a more selective NO_2 measurement to that provided by molybdenum catalysts (Ridley et al., 1988; Ryerson et al., 2000). The conversion efficiency is determined by Eq. (2) where t is the residence time within the photolysis cell. Here k[Ox] is the concentration and rate constant of any oxidant that reacts with NO to form NO_2 (Ryerson et al., 2000).

$$\mathrm{CE} = \left[\frac{jt}{jt + k\,[\mathrm{Ox}]\,t}\right]\left[1 - \exp^{(jt - k[\mathrm{Ox}]t)}\right] \quad (2)$$

The rate constant of photolysis of NO_2 (j), and so, the rate of production of additional NO beyond that in the original sample is given in Eq. (3).

$$j(T) = \int_{\lambda\,\mathrm{min}}^{\lambda\,\mathrm{max}} F(\lambda)\,\sigma(\lambda, T)\,\phi(\lambda, T)\,\mathrm{d}\lambda \quad (3)$$

In Eq. (3) j is the rate constant (s^{-1}), F is the spectral photon flux (photons $cm^{-2}\,s^{-1}\,nm^{-1}$), σ is the absorption cross section of NO_2 (cm^2), ϕ is the quantum yield (dimensionless) of NO_2 photo-dissociation, and T is the temperature (Sander et al., 2011). The j value of the converter is practically determined by the irradiant photolysis power of the UV emitting elements and how efficiently the power is used.

2.2.1 Standard BLC

Standard BLCs consist of two ends housing the UV-LEDs (1 W, 395 nm, UV Hex, Norlux Corp) within a heat sink to which is attached a cooling fan. The ends are bolted to a central section with rubber gaskets forming an air-tight seal. Within the centre section

ACPD
15, 28699–28747, 2015

a propriety Teflon-like material block is housed which serves as a highly UV reflective (> 0.95) cavity thought which the sample gas flows (Buhr, 2007). On two of the opposing sides of the centre section are 1/4 inch Swagelok fittings acting as an inlet and outlet for the sample gas.

The volume of this illuminated sample chamber is 16 mL which, with a standard flow rate of 1 standard L min^{-1}, gives a sample residence time of 0.96 s. Additional lamp end units were also supplied by AQD.

The conversion efficiency of the standard BLC with a sample flow of 1 standard L min^{-1} was 22 to 42 % (j = 0.2...0.6 s^{-1}) depending on the combination of lamp units used whilst the external temperature of the converter was typically 34 to 45 °C. All experiments were carried out at with sample gas at ambient temperature and pressure; 20 °C, 1 atm.

2.2.2 High power BLC

The high power BLC of the aircraft instrument is designed to operate at a higher flow rate (1.5 standard L min^{-1}), lower pressure (~ 300 Torr) and therefore lower residence time, to that of the standard BLC to allow fast time resolution measurements from an aircraft. For this reason a greater number (six) of more powerful UV-LEDs [2 W, 395 nm, Nichia Corp] are used in order that the conversion efficiency be acceptable under these conditions. The lamps are placed evenly along two sides of a cylindrical cavity of the same highly UV reflective Teflon with inlets at opposing ends. The high power BLC lamps are actively (Peltier) cooled to 47 °C and without Peltier cooling reach 77 °C. It was therefore possible to control the internal temperature of the BLC by varying the power supplied to the Peltier elements via the temperature controller.

The volume of this illuminated sample chamber is 10 mL which, with a standard flow rate of 1 standard L min^{-1}, gives a sample residence time of 0.60 s resulting in a conversion efficiency of 93 % (j = 6.5 s^{-1}).

ACPD
15, 28699–28747, 2015

2.3 TD-LIF analyser

Laser induced fluorescence (LIF) provides a direct NO_2 measurement, as opposed to chemiluminescence with conversion. A direct method of NO_2 determination to compare with the BLC NO_2 converters is desirable in order to properly know the source of any "artefact" NO_2 signal.

The Thermal Dissociation Laser Induced Fluorescence (TD-LIF) system is a custom instrument developed for aircraft and ground-based observations of NO_2, $\sum$PNs, $\sum$ANs, and HNO_3. A detailed description of the TD-LIF instrument can be found in Di Carlo et al. (2013), with a short description given here. It uses laser induced fluorescence (LIF) to detect NO_2 concentrations directly (Dari-Salisburgo et al., 2009; Matsumoto and Kajii, 2003; Matsumoto et al., 2001; Thornton et al., 2000) and, coupled with a thermal dissociation inlet system, allows measurement of peroxy nitrates ($\sum$PNs), alkyl nitrates ($\sum$ANs), and HNO_3 after conversion into NO_2 (Day et al., 2002). The TD-LIF comprises four main parts: the laser source, the detection cells system, the inlet system and the pumps. The laser source is a Nd:YAG pulse doubled laser (Spectra-Physics, model Navigator I) that emits light at 532 nm with a power of 3.8 W, a repetition rate of 15 kHz and 20 ns pulse-width. The detection cells system comprises four identical cells, one for each compound class, to allow simultaneous measurements. Each cell is formed by a cube and two arms where the laser beam passes through the sample air flow in the centre of the cell. Perpendicular to both (laser beam and air flow) there is the detector that is a gated photomultiplier with lens and long pass filters to optimize the fluorescence detection, minimizing the non-fluorescence light that reaches the detector (Di Carlo et al., 2013; Dari-Salisburgo et al., 2009). The pump system includes a roots blower coupled to a rotary vane pump to maintain a flow of 6 L min^{-1}. The common inlet system is split in four channels: one at ambient temperature to measure NO_2, and the last three heated at 200, 400 and 550 °C, to thermally dissociate $\sum$PNs, $\sum$ANs, and HNO_3 respectively into NO_2 (Di Carlo et al., 2013). To minimize quenching due to atmospheric molecules, and therefore increase the sen-

ACPD
15, 28699–28747, 2015

sitivity of the TD-LIF, each cell is kept at low pressure (3–4 Torr). This increases the fluorescence lifetime and facilitates the time-gating of the photomultiplier to further reduce the background (Dari-Salisburgo et al., 2009). The TD-LIF is routinely checked for background by an over-flow of zero air in the detection cells; and calibrated by standard addition of known amount of NO_2 from a cylinder (NIST traceable) diluted in zero air – the flow of both zero air and NO_2 being MFC controlled. The time resolution of the measurements is 10 Hz and the detection limits are: 9.8, 18.4, 28.1, and 49.7 pptv (1 s, $S/N = 2$) for NO_2, $\sum$PNs, $\sum$ANs, and HNO_3 cells, respectively (Di Carlo et al., 2013).

2.4 PAN preparation

In order to test the sensitivity of the instrument to peroxy-acetyl nitrate interferences it was prepared by the photolysis in air of acetone and NO as described by (Meyrahn et al., 1987) and later by (Warneck and Zerbach, 1992; Zellweger et al., 2000). Reactions (R9)–(R11) describe the mechanism by which PAN is formed from acetone photolysis.

$$(CH_3)_2CO + O_2 + h\nu \rightarrow CH_3C(O)O_2^{\bullet} + CH_3^{\bullet} \quad \text{(R9)}$$

$$CH_3C(O)O_2^{\bullet} + NO \rightarrow CH_3C(O)O^{\bullet} + NO_2 \quad \text{(R10)}$$

$$CH_3C(O)O_2^{\bullet} + NO_2 \rightarrow CH_3C(O)O_2NO_2 \quad \text{(R11)}$$

Here NO_2 reacts stoichiometrically with the acyl radical to form PAN. In practice, an excess of acetone is used to ensure that NO reacts completely. A minor product also found in the photolysis of acetone is methyl nitrate, $MeONO_2$, which is typically approximately 1 % of the total yield (Mills et al., 2007). The proposed origin of the methyl nitrate is shown in Reactions (R12)–(R16). Methyl nitrate is also found in the atmosphere through oceanic emission (Moore and Blough, 2002) and as a product of the thermal decomposition of PAN (Fischer and Nwankwoala, 1995; Roumelis and Glavas, 1992; Warneck and Zerbach, 1992). Reactions (R15), (R17) (Fischer and Nwankwoala, 1995) show that the formation of nitro-methane and HONO is also possible from PAN

ACPD
15, 28699–28747, 2015

synthesis by acetone photolysis.

$$2CH_3C(O)O_2^{\bullet} \rightarrow 2CH_3CO_2^{\bullet} + O_2 \quad \text{(R12)}$$

$$CH_3CO_2^{\bullet} \rightarrow CH_3^{\bullet} + CO_2 \quad \text{(R13)}$$

$$CH_3^{\bullet} + CH_3C(O)O_2^{\bullet} \rightarrow CH_3O^{\bullet} + CH_3CO_2^{\bullet} \quad \text{(R14)}$$

$$(CH_3^{\bullet} + NO_2 \rightarrow CH_3NO_2) \quad \text{(R15)}$$

$$CH_3O^{\bullet} + NO_2 \rightarrow CH_3ONO_2 \quad \text{(R16)}$$

$$(CH_3O^{\bullet} + NO_2 \rightarrow HCHO + HONO) \quad \text{(R17)}$$

A dedicated "PAN generator", as used by Whalley et al. (2004), was employed to produce a consistent source of PAN. The generator consists of: flow control elements for the NO standard gas, the acetone flow, and the zero air diluent flow; an acetone permeation oven consisting of a reservoir of HPLC grade acetone (ACS grade, Acros) with a silicone permeation tube placed in the headspace through which zero air flows, all thermo-stated at 30 °C; and a Pyrex glass photolysis cell illuminated by UV light centred at 285 nm (Pen-Ray mercury lamp, UVP). The Pyrex functions to filter wavelengths below 290 nm within the photolysis cell thus minimizing PAN photolysis (Mills et al., 2007).

All flow rates within the PAN generator were calibrated using a Gilian Gilibrator-2 Air Flow Calibrator (Sensidyne). The PAN generator is capable of continuously producing 0.1–20.0 ppbv PAN. Linearity and mixing ratio of the PAN output was confirmed by PAN-GC equipped with an ECD detector as described by Whalley et al. (2004), and also by complete reduction back to NO using a heated (325 °C) molybdenum catalyst (Thermo Environmental). A Laser Induced Fluorescence instrument, described in Sect. 2.2.3, was used to find if any NO_2 produced directly in the PAN generator with the results presented in Sect. 2.4.1.

ACPD
15, 28699–28747, 2015

2.5 Zero air

Zero air was generated from dried (−40 °C dew point) compressed air by subsequent filtering through a cartridge of molecular sieve (13×, Sigma Aldrich) to ensure a consistent humidity throughout all experiments and was regenerated by heating to 250 °C for 24 h when necessary. A second filter cartridge placed after the molecular sieve was packed with Sofnofil (Molecular Products) and activated charcoal (Sigma Aldrich) in order to remove ozone, NO_x and volatile organic compounds (VOC) which may be present in the compressed air. Zero air generated from the compressed air and filter cartridges system and zero air from an Eco Physics AG PAG 003 pure air generator (the industry standard) were both sampled by the NO chemiluminescence analyser. No difference in the counts of the NO analyser was observed between the two sources of zero air. Thus the NO content of both sources of zero air was considered to be comparably low.

The NO_2 content of any zero air used is critical (more so than NO) in this study. In order to determine the NO_2 content of the zero air sources a direct measurement of NO_2 was required in order to avoid biasing the experimental procedure. The LIF instrument described in Sect. 2.2.3 was used to compare the zero air sources (Table 1).

Zero air from both PAG 003 and filter stack was sampled by the NO_2 LIF analyser. Additionally, high grade bottled zero air (BTCA 178, BOC Specialty Gasses) was analyzed for NO_2. Table 1 shows the photomultiplier counts per second whilst sampling 1.5 standard L min^{-1} of zero air. The dark counts of the PMT in the absence of laser light are typically less than 3 counts s^{-1}. The counts recorded are therefore the sum of any NO_2 fluorescence and scattered laser light. It is clear that the Sofnofil/Carbon filter system has an advantage over both the PAG 003 and BTCA 178 zero air sources in that a lower signal for NO_2 fluorescence was observed. Typical sensitivity of the LIF NO_2 channel was ∼ 180 cps ppb^{-1}, thus a 4–4.5 cps improvement in zero background equates to 22–25 ppt s improvement in accuracy. Consequently, all dilution, zeroing, and PAN generation utilized the Sofnofil/Carbon filter system.

ACPD
15, 28699–28747, 2015

2.6 Experimental procedure

The NO_x analysers were first calibrated for sensitivity/converter efficiency and sampling zero air by overflowing the inlet from the internal source prior to the experiment for at least 2 h. This is because the PAN from the generator is in zero air which has a very low dew point and the sensitivity of the NO_x analyser is reduced by high humidity in the sample. This means that switching the NO_x analyser from sampling ambient (humid) air to zero air causes the sensitivity to rise slowly and the humidity inside of the reaction cell to decrease. After establishing an NO flow (4.78 ppm NO in N_2, BOC specialty gases) of 0.5 mL min^{-1} into the PAN generator, the acetone flow was then adjusted to ~ 10 mL min^{-1} and the diluent flow of zero air adjusted to achieve the desired output mixing ratio. The internal zero air of the NO_x analyser was then shut off so that the NO_x analyser was sampling zero air from the PAN generator. Note that the total flow from the PAN generator always exceeded the sample requirements of the NO_x analyser with excess flow vented to the atmosphere. The system was then allowed to stabilize until a stable NO value was recorded on the NO_x analyser. Next, the acetone photolysis lamp of the PAN generator was switched on so that acetone was photolysed in the presence of NO to form PAN. Complete NO conversion to PAN was indicated by the fact that in all cases the NO signal measured by the NO_x analyser fell to ~ 0 ppbv after the acetone/NO mixture was illuminated by the photolysis lamp. The diluent flow from the PAN generator was then varied to achieve PAN mixing ratios of between 0.2 to 1.3 ppbv. The corresponding NO_2 signal was recorded once stable. This procedure was repeated for various combinations of BLC lamps/assemblies and analyser operation modes.

In order to investigate any interference from unreacted acetone, the NO_x analyser was allowed to sample the output of the PAN generator with the photolysis lamp off i.e. a flow of acetone and NO gas. No additional signal relative to zero air during the NO or NO_2 measurement cycle was observed during these experiments at any mixing ratio.

ACPD
15, 28699–28747, 2015

To investigate any interference from unreacted peroxy radicals left over from photolysis of excess acetone, produced in Reaction (R6), the NO_x analyser was allowed to sample acetone that had been photolysed within the PAN generator in the absence of NO. NO was added downstream of the photolysis cell also. No additional signal over zero air during the NO or NO_2 measurement cycle was observed in either case, photolysed acetone with or without nitric oxide addition. Thus, it was concluded that acetone does not interfere within the BLC and that peroxy radicals do not exist outside of the broadband photolysis cell of the PAN generator. It should be noted that sampling acetone does cause an increase in the zero count of the NO_x analyser as acetone does react with ozone; this chemiluminescence interference is known (Dunlea et al., 2007) and is accounted for in the measurements.

To test whether the PAN generator produced any NO_2 directly (i.e. rather than as a consequence of conversion of PAN to NO_2), a direct measurement of NO_2 was employed using the TD-LIF described in Sect. 2.2.3. The measured signal relative to pure zero air was measured in the LIF NO_2 channel when sampling various mixing ratios of PAN from the generator as shown in Fig. 1. It is evident that the NO_2 signal observed while sampling PAN from the generator lies within the noise of the zero signal measurement. In this case each point represents a 10 min average as does the zero measurement. With an averaging time of 10 min the theoretical limit of detection is estimated to be less than 0.1 pptv – taking a 10 Hz LOD of 9.8 pptv, and averaging 6000 points (i.e. 10 min) the precision improves by a factor of approximately $1/n$ where n is the number of points averaged (Lee et al., 2009). It is therefore conservatively estimated that less than 1 ppt NO_2 at 1000 ppt PAN (0.1 %) is produced by the PAN generator. This is less than previously estimated (Mills et al., 2007), albeit at higher PAN mixing ratios and lower residence times within the acetone photolysis cell with the same generator.

It was therefore determined that only PAN could be an interfering species in the BLC from the PAN generator. The small percentage of methyl nitrate which may be produced is discounted due to it being less thermally labile that PAN itself. Additionally, the percentage interference observed is significantly greater than any expected or

ACPD
15, 28699–28747, 2015

reported methyl nitrate yield from PAN synthesis by acetone photolysis i.e. 1 % (Mills et al., 2007). In the following discussion we address the possibility of photolytic and thermal dissociation of PAN or methyl nitrate to NO_2 and subsequently NO within the photolytic convertor.

2.7 Residence time

The residence time of PAN in the 2.7 m PFA inlet linking the PAN generator to the NO_x analyser was varied by varying the flow rate. This was achieved by altering the sample flows through the each of the NO_x analyser channels (which share a common inlet).

3 Impact of PAN on NO_2 measurements

In this section we discuss experiments investigating the potential impact of PAN on the two NO_2 instruments. In Sect. 3.1 and 3.2 we explore the interference in the laboratory instrument with a range of BLC convertors, eliminating any possibility for inlet effects in Sect. 3.3, and in Sect. 3.4 we explore the interference in the aircraft instrument which has an active cooling of the convertor. In Sect. 3.5 we investigate whether photolytic decomposition of PAN could lead to the interferences and in Sect. 3.6 we investigate whether thermal decomposition could be the source.

3.1 Standard BLC and laboratory NO_x analyser in constant mode

PAN was introduced to the NO_x analyser, equipped with a BLC as described in Sect. 2.2.1, diluted in zero air through a range of mixing ratios. The resulting mixing ratio recorded by the analyser was recorded and is presented in the following sections. Figure 2 shows that the NO_2 signal is proportional to increasing PAN mixing ratios. The measured mixing ratios of NO_2 were 8–25 % of the initial PAN mixing ratio.

ACPD
15, 28699–28747, 2015

The percentage conversion of PAN to NO_2 is on average highest at the lowest converter efficiency and vice versa. Potential reasons for this effect are addressed in Sect. 3.6.

3.2 Standard BLC and laboratory NO_x analyser in switching mode

Figure 3 shows the NO_2 signal resulting from the same three BLC units operated in switching mode (40 % duty cycle). The percentage PAN conversion observed is lower in all cases than in the corresponding constant mode. This is likely due to the lower lamp temperature as a result of operating only 40 % of the time. The relationship between conversion efficiency and signal are not as clearly evident here as for constant mode operation (Fig. 2). It is possible that the greater variation in the measurement due to the lower amounts of NO_2 produced obscured any trend, however it is clear that there is still a significant proportion of PAN measured as NO_2; an average of 5.8 %.

3.3 Inlet residence time effects

It is not clear from either Fig. 2 or 3 whether the PAN decomposition occurs within the BLC exclusively or within the inlet of the system, as has been claimed previously (Fehsenfeld et al., 1987). Previous studies (Fehsenfeld et al., 1990; Ridley et al., 1988; Sadanaga et al., 2010) have also reported a small PAN interference with photolytic converters, while some found the contribution to the NO_2 signal from PAN to be negligible (Ryerson et al., 2000). Others (Val Martin et al., 2008) acknowledge the possibility for an interference and estimate a small (2 to 4 pptv) positive bias. The photolytic converter designs in the aforementioned studies vary greatly in their implementation and do not have the same ubiquity as BLCs used here, i.e. within the GAW network (Penkett et al., 2011).

Table 2 demonstrates that the residence time of PAN within the inlet does not affect the signal arising from PAN decomposition in our system. This rules out any significant contribution from the inlet to PAN decomposition. The inlet in this case consists of ca.

ACPD
15, 28699–28747, 2015

2.7 m 1/4 inch PFA tubing shielded from light and held at 20 °C. In other applications, for example if the inlet is heated, contaminated, or has a very long residence time, it is quite possible that significant PAN decomposition occurs.

From these experiments it is evident that a significant NO_2 signal is observed when sampling PAN diluted in zero air. The signal seen corresponds to around 5 to 25 % of the PAN supplied which represents a significant interference. The possibility of thermal decomposition within the inlet was ruled out.

3.4 High powered and actively cooled photolytic NO_2 converter

Figure 4 shows the difference in NO_2 signal between the cooled and uncooled high powered BLC described in Sect. 2.2.2. In all of the cooled cases the NO_2 measured was significantly lower than in the uncooled case; this accounts for any increased artefact (the signal recorded when sampling zero air) in the uncooled case. The conversion efficiency was 93 % for $NO_2 \rightarrow NO$.

The effect of actively cooling the BLC lamps is significant as apparent in the much lower NO_2 concentrations measured whilst sampling a range of PAN mixing ratios (Fig. 4). It is therefore plainly evident that there is a significant effect of cooling the UV-LEDs which acts to mitigate any signal arising from PAN.

3.5 Possible photolytic interferences of BLCs

Spectral radiograms of the UV-LED elements of standard BLCs were obtained using an Ocean Optics QE65000 spectral radiometer coupled to a 2π quartz collector. The spectrometer and collector optics were calibrated using an NIST traceable light source (OL FEL-A, Gooch and Housego) and ultra-linear power supply (OL 83A, Gooch and Housego). The light source is a 1000 W quartz-halogen tungsten coiled-coil filament lamp with spectral irradiance standard F-1128. The lamp was operated at 8 Amps DC (125 V), with the lamp-collector distance fixed at 50 cm. Calibration was carried out in

ACPD
15, 28699–28747, 2015

a light sealed chamber. Spectra of the BLC UV-LED lamps were taken within the same light-proof chamber with the same distance between the lamp and collector.

Figure 5 shows the spectral emission of six different BLC UV-LED units. These units ranged in age from new to nearing the end of their service life i.e. the conversion efficiency of the whole BLC unit had fallen below acceptable limits. As the LED units age, the relative intensity of their outputs declines, this decrease in intensity can be due to dimming of the overall output, or failure of individual array elements determined by visual inspection during operation. It should be pointed out however, that the light intensity of the UV-LEDs is not directly proportional to the NO_2 conversion efficiency of the complete whole BLC. Rather, the conversion efficiency is strongly dictated by the condition of the reflective Teflon-like cavity. For example, disabling one of the two lamps in a BLC does not reduce the conversion efficiency by half, but by a much smaller percentage. Additionally, replacing the UV-LED elements of a converter whose conversion efficiency has dropped below 30 % with new lamps will not lead to a recovery of the conversion. Scrupulous cleaning of the reflective cavity with solvent and mild abrasion of the surface will however recover the conversion efficiency considerably.

Figure 6 depicts the absorption cross sections of atmospheric nitrogen compounds against the measured spectral output of UG5 UV-passing filter glass (Schott, 1997) used in lamp-type PCL optics e.g. Eco Physics PCL 762, and the averaged measured spectral output of six individual BLC UV-LED arrays of varying running hours. Also shown is the NO_2 quantum yield (Gardner, 1987; Koepke et al., 2010). It can be discerned that the UV-LED output overlaps fully with the NO_2 absorption band and the NO_2 quantum yield and is therefore photon efficient. It is also shown that there in minimal overlap with HONO and no overlap in the spectrum at all with PAN. It has been shown (Carbajo and Orr-Ewing, 2010; Talukdar et al., 1997) that there is no overlap either with methyl, ethyl or isopropyl nitrate – methyl nitrate being a minor impurity in PAN synthesis. There is only very minor overlap in the PCL optics spectrum with PAN, methyl ethyl, and isopropyl nitrate. There is a great deal of overlap with HONO which

ACPD
15, 28699–28747, 2015

the UV-LEDs do not possess however. Both systems suffer some overlap with NO_3 radicals and $BrONO_2$, more so in the case of PCL optics than for UV-LEDs.

3.6 Possible thermal interferences in BLCs

The thermal and electronic characteristics of the standard BLC lamps were ascertained in bench tests and are summarized in Table 3. Each lamp was run constantly on the bench whilst recording the surface temperature and power draw of the light emitting element. The surface temperature was recorded once a stable maximum had been reached and maintained for at least 10 min – representative of using a BLC in constant mode. The ambient temperature during the experiments was 20 °C.

Table 3 details the power draw and surface temperature of three BLC UV-LED lamp pairs measured during tests, along with their $NO_2 \rightarrow NO$ convertor efficiencies when assembled as a complete BLC. The surface temperature of the individual lamps correlate positively with the power drawn by each lamp ($R^2 = 0.96$) and indeed with output intensity (Fig. 2), but with each lamp pair there is only weak correlation ($R^2 = 0.43$) between converter efficiency and temperature. It is worth noting that the power consumption is a combination of the light output, heat dissipation, and power to the cooling fan. It is clear however that the temperature experienced by the sample gas within the NO_2 converter is significantly above ambient. In fact, the entire NO_2 conversion cavity is heated by the lamps leading to external temperatures of the converter of between 34 and 45 °C.

It is known that the major product from thermal decomposition of PAN is NO_2; Reaction (R18) (Roumelis and Glavas, 1992; Tuazon et al., 1991). The NO_2 produced thermally within the converter may then be photolysed to NO and thus be measured as NO_x and attributed to atmospheric NO_2.

$$CH_3C(O)OONO_2 \rightleftharpoons CH_3C(O)OO^{\bullet} + NO_2 \qquad \text{(R18)}$$

A model of the thermal decomposition of PAN over a range of temperatures within the BLC with a residence time of 0.96 s is shown in Fig. 7. The model run was conducted

ACPD
15, 28699–28747, 2015

in Facsimile using rate constants from IUPAC Evaluated Kinetic Data (Atkinson et al., 2006).

The model output indicates that measureable PAN decomposition to NO_2 occurs above ca. 50 °C. At the maximum LED surface temperature recorded (80 °C) the model predicts ca. 30 % decomposition of PAN to NO_2. However, as only the two UV-LED lamps are at such an elevated temperature we can expect a temperature gradient/heating rate within the BLC so that the average temperature seen by the sample gas over the 0.96 s residence is somewhat lower. Also, it is expected that in a switching mode with only 40 % duty cycle of the lamps, their surface temperature would be lower also. This is borne out when using the external surface temperature of the BLC as a proxy – the temperature was lower in switching mode than in constant mode for the same conversion efficiency. It is shown more clearly in the inset that an average temperature of 60 °C would cause a 4.6 % decomposition of PAN and account for the NO_2 measured during experiments with the standard BLCs. Therefore, together with the spectral measurements reported in Sect. 3.5, it seems highly unlikely that the source of the artefact signal is through direct photolysis of PAN, leaving thermal decomposition modelled in Fig. 7 the remaining explanation.

In Sect. 3.1 the percentage conversion of PAN to NO_2 was found to be, on average, highest at the lowest converter efficiency and vice versa. The fact that the convertor temperatures are very similar at different convertor efficiencies (Table 3) suggests that the percentage of PAN thermally dissociated in each case is similar. Explanation for the inverse relationship between percentage conversion of PAN to NO and conversion efficiency (Fig. 2) lies in the way that the NO_2 concentration is derived, which is an inverse function of the assumed conversion efficiency as in Eq. (2) where converter efficiency is expressed fractionally. If in fact the conversion efficiency of PAN to NO in the convertor was not related to the measured NO_2 to NO conversion efficiency but instead a constant value, then the apparent relationship between CE and % conversion would disappear. This explanation is consistent with the fact that when the average conversion percentage in Fig. 2 is normalized to conversion efficiency, the percentage

ACPD
15, 28699–28747, 2015

for the three BLCs is remarkably similar (Table 4) with the average PAN decomposition of 4.6 % needed to produce the spurious signal observed.

Above a threshold temperature of 25 °C, the NO_2 formed in Reaction (R18) may be excited through the dissipating of internal energy from the parent PAN molecule (Mazely et al., 1995), this NO_2^* is then more readily photolysed to NO within the BLC than ground state NO_2. The discussion above suggests that a similar proportion of the NO_2 evolved from thermal dissociation of PAN is converted to NO within the BLC leading to the apparent inverse correlation between conversion efficiency and PAN "artefact". Consequently, the lower $NO_2 \rightarrow NO$ conversion efficiency of a BLC, the greater the positive error in NO_2 when PAN is present.

4 Atmospheric implications

We have shown that a significant proportion of PAN can be decomposed under the normal operating conditions of a BLC equipped NO chemiluminescence instrument leading to a spurious increase in measured NO_2 of 5 to 20 % of the PAN supplied. The UV-LED light source employed by was found to reach a temperature of 56 to 80 °C in normal operation with the surface temperature correlating positively with power draw and output intensity.

The positive bias in NO_2 measurements by NO chemiluminescence using BLCs has implications for data in both remote background sites and polluted areas. Figure 8 shows the thermal decomposition profiles of many common NO_y species. Whereas only a small fraction of PAN is found to convert to NO_2 at the operating temperatures ($\sim$ 5 % at 60 °C) of the instrument, a number of more thermally labile compounds exist which become more important at higher latitudes and altitudes.

The degree of thermal decomposition within the instrument will depend upon the thermal profile of the air ($T(t)$) as it passes through the instrument. This can be parameterized as a relaxation timescale (τ s) for temperature from the ambient temperature

ACPD
15, 28699–28747, 2015

(T_0) to that of the BLC (T_{BLC}) as in Eq. (4).

$$T(t) = T_0 + (T_{BLC} - T_0)\exp\left(-\frac{t}{\tau}\right) \quad (4)$$

The rate at which thermal equilibrium is reached within the cell, τ, is calculated as 0.42 s from the observed PAN decomposition of 4.6 % (from which $T(t)$ is derived), at 20 °C ambient temperature, a BLC temperature of 75 °C and a 1 s residence time. This allows a calculation of the potential interference from other thermally labile NO_y compounds.

Given a 1st order loss of the PAN like compound and a temperature profile within in the instrument as described in 4 we have 5:

$$\frac{\mathrm{d[PAN]}}{\mathrm{d}t} = -k(T)[\mathrm{PAN}] = -k(t)[\mathrm{PAN}] \quad (5)$$

Given the laboratory observations of the temperature dependence of the rate constant (typically $k(T) = A\exp(-B/T)$), and the parameterized temperature within the instrument ($T(t)$), the fraction of the compounds that will have decomposed can be found by numerical integration.

Figure 9 uses output from the GEOS-Chem model (version 9.3, http://www.geos-chem.org, Bey et al., 2001) run at 2° × 2.5° resolution, plus updates described in Sherwen et al. (2015), to provide an estimate of the interference on NO_2 from the decomposition of NO_y species within a BLC photolytic converter. The species used for this analysis are: PAN; MPAN; PPN; $IONO_2$; $BrONO_2$; $ClONO_2$; N_2O_5; $CH_3O_2NO_2$, HO_2NO_2. Thermal decomposition information are taken from IUPAC evaluated kinetic data (Atkinson et al., 2003, 2006, 2007). Interferences are calculated for each month of a one year simulation and the maximum value shown. The estimate assumes a BLC conversion efficiency of 100 % $NO_2 \rightarrow NO$ and thus does not include the extra signal from the photolysis of $NO_2^* \rightarrow NO$ with converters where conversion is less than unity – in this case a multiplying factor exists.

ACPD
15, 28699–28747, 2015

Figure 9 shows that in extreme circumstances NO_2 may be over-reported by many hundreds of percent. These are in regions that typically have low NO_x concentrations and are cold (polar), and in the upper troposphere. Here, compounds such as PAN and HO_2NO_2 are in high concentrations compared to NO_x and it is not surprising that thermal decomposition can have an impact. Upper tropospheric over estimates of NO_2 concentrations could be as high as 150 pptv.

The NO_2 bias shown in Fig. 9 impacts the modelled Leighton ratio. In Fig. 10 the model is sampled every daylight hour for every surface grid box for the month of March. The calculation shown in red is the Leighton ratio calculated from the modelled concentrations of NO, NO_2, jNO_2, O_3, T, HO_2, RO_2, BrO and IO. The model value is in general close to 1. In the blue the same calculation is performed but including the interferences on the NO_2 channel from the instrumental decomposition of a range of BLC lamp temperatures between 60 and 105 °C (described by τ of 0.42 s and a residency time of 1 s). Here there are significant interferences.

As shown in Fig. 10 the Leighton ratio can be extremely perturbed from what would be predicted by all available measurements given the NO_2 bias we have shown exists with photolytic NO_2 converters which operate above ambient temperature. This is especially true in low NO_x environments. This has led to either hypothesizing (a) an unknown, unmeasured, selective oxidant "compound *X*" or, (b) theoretical mechanisms by which NO is converted to NO_2 (Bauguitte et al., 2012; Cantrell et al., 2003; Frey et al., 2013, 2015; Hosaynali Beygi et al., 2011).

As a practical example with an analogous system to that used in this study, the NO_x observations of Hosaynali Beygi et al. (2011) taken in the South Atlantic during the "OOMPH" project (Ocean Organics Modifying Particles in both Hemispheres) serve as a case study. During this cruise a BLC photolytic NO_2 converter (Droplet Measurement Technologies, Colorado, USA), with a residence time of 1 s, as described in this study – coupled to an NO chemiluminescence analyser was deployed aboard the French research vessel Marion Dufresne II. The cruise track covered the South

ACPD
15, 28699–28747, 2015

Atlantic Ocean from Cape Town, South Africa to Punta Arenas, Chile, reaching 60° S during March 2007.

The results presented by Hosaynali Beygi et al. (2011) show an NO_2 : NO ratio which is a factor c.a. 7 greater than can be explained given the available supporting observations of O_3, CO, OH, HO_2, RO_x ($RO + RO_2 + HO_x$), i.e. measured NO_2 is much greater than the Leighton relationship would predict. This apparent Leighton ratio is attributed by the author to an "unknown oxidant" which selectively converts NO to NO_2.

The authors estimate a minimal photolytic interference from atmospheric nitrates using their BLC, consistent with our analysis (Sect. 3.5 and Fig. 6). Only PAN decomposition within the inlet line is considered as a potential interference, but is estimated to be minimal (< 7 ppt) due to the low ambient temperature range of 3 to 11 °C. Our results have shown that thermal, rather than photolytic decomposition of atmospheric NO_y species with the converter itself is the major source of over-reporting in NO_2 measurements made with BLCs. Indeed, our model study predicts interference of 50 to 100 % in the region of the cruise, assuming an NO_2 converter efficiency of 100 %, whereas in the OOMPH observations the efficiency was 59 % thus, a multiplying factor may apply to any PAN interference of ~ 1.7.

Presented in Fig. 4 of Hosaynali Beygis' paper on page 8503 (Hosaynali Beygi et al., 2011) is the Leighton ratio calculated from their NO_2 data and ancilarry measurments. The ratio in the pristine background appears to be significantly biased towards NO_2, exceeding what the authors are able to explain given their measurments of HO_x, RO_x and OH. Their values fit well within the modelled Leighton ratios shown in Fig. 10 when an instrumental bias is included however. This is suggestive of an instrumental NO_2 bias cause by a BLC with a lamp temperature of around 90 °C, however does not include any multiplying effect of having an NO_2 conversion efficiency less than unity. As the efficiency is 59 % the actual temperature would not necessarily be so high as 90 °C. Eliminating this NO_2 over-reporting closes the oxidative balance implied by their other data and removes the need to invoke any compound *X* or mystery oxidant.

ACPD
15, 28699–28747, 2015

5 Conclusions

Measurements of NO_2 collected using photolytic converters and chemiluminescence systems may be significantly biased in low NO_x environments. Thermal decomposition of NO_y species within the NO_2 converter produces spuriously high readings; this is especially true in pristine environments and at high elevations where the NO_y to NO_x ratio may be high. Over-reporting of NO_2 has been shown to lead to apparent gaps in oxidation chemistry which cannot be explained with any available measurements. This has led to theorization of an unknown "compound *X*" which selectively oxidizes NO to NO_2, however this is likely anomalous and simply due to error in the NO_2 determination.

In order to mitigate this overestimation of the NO_2 mixing ratio by the dissociation of PAN and other compounds it is desirable to have the highest possible $NO_2 \rightarrow NO$ conversion efficiency, i.e. unity, to mitigate the multiplying effect of having lower conversion efficiencies. High conversion efficiency is now achievable thanks to advancements in the power density of UV-LEDs currently available; new generation BLCs have a CE > 95 % for example. Additionally, actively cooling the UV emitting elements or separating them from the gas stream is essential in order that the sample gas should not contact any surface which is above ambient temperature. Failure to achieve this may result in spuriously high NO_2 observations.

Acknowledgements. The authors would like to express their gratitude to Stephane Bauguitte of FAAM for their scientific discussion, and Lisa Whalley of Leeds for the PAN generator and spectral radiometer/calibration equipment. The financial support of NCAS, the National Centre for Atmospheric Science, and of NERC, the Natural Environmental Research Council for supporting the studentship of Chris Reed is gratefully acknowledged.

References

Ainsworth, E. A., Yendrek, C. R., Sitch, S., Collins, W. J., and Emberson, L. D.: The effects of tropospheric ozone on net primary productivity and implications for climate change, Annu. Rev. Plant Biol., 63, 637–661, doi:10.1146/annurev-arplant-042110-103829, 2012.

ACPD
15, 28699–28747, 2015

Ashmore, M. R.: Assessing the future global impacts of ozone on vegetation, Plant Cell Environ., 28, 949–964, doi:10.1111/j.1365-3040.2005.01341.x, 2005.

Atkinson, R., Baulch, D. L., Cox, R. A., Crowley, J. N., Hampson, R. F., Hynes, R. G., Jenkin, M. E., Rossi, M. J., and Troe, J.: Evaluated kinetic and photochemical data for atmospheric chemistry: Volume I – gas phase reactions of O_x, HO_x, NO_x and SO_x species, Atmos. Chem. Phys., 4, 1461–1738, doi:10.5194/acp-4-1461-2004, 2004.

Atkinson, R., Baulch, D. L., Cox, R. A., Crowley, J. N., Hampson, R. F., Hynes, R. G., Jenkin, M. E., Rossi, M. J., Troe, J., and IUPAC Subcommittee: Evaluated kinetic and photochemical data for atmospheric chemistry: Volume II – gas phase reactions of organic species, Atmos. Chem. Phys., 6, 3625–4055, doi:10.5194/acp-6-3625-2006, 2006.

Atkinson, R., Baulch, D. L., Cox, R. A., Crowley, J. N., Hampson, R. F., Hynes, R. G., Jenkin, M. E., Rossi, M. J., and Troe, J.: Evaluated kinetic and photochemical data for atmospheric chemistry: Volume III – gas phase reactions of inorganic halogens, Atmos. Chem. Phys., 7, 981–1191, doi:10.5194/acp-7-981-2007, 2007.

Bauguitte, S. J.-B., Bloss, W. J., Evans, M. J., Salmon, R. A., Anderson, P. S., Jones, A. E., Lee, J. D., Saiz-Lopez, A., Roscoe, H. K., Wolff, E. W., and Plane, J. M. C.: Summertime NO_x measurements during the CHABLIS campaign: can source and sink estimates unravel observed diurnal cycles?, Atmos. Chem. Phys., 12, 989–1002, doi:10.5194/acp-12-989-2012, 2012.

Bridier, I., Caralp, F., Loirat, H., Lesclaux, R., Veyret, B., Becker, K. H., Reimer, A., and Zabel, F.: Kinetic and theoretical studies of the reactions $CH_3C(O)O_2 + NO_2 + M \Leftrightarrow CH_3C(O)O_2 + M$ between 248 and 393 K and between 30 and 760 torr, J. Phys. Chem., 95, 3594–3600, doi:10.1021/j100162a031, 1991.

Brown, S. S., Dibb, J. E., Stark, H., Aldener, M., Vozella, M., Whitlow, S., Williams, E. J., Lerner, B. M., Jakoubek, R., Middlebrook, A. M., DeGouw, J. A., Warneke, C., Goldan, P. D., Kuster, W. C., Angevine, W. M., Sueper, D. T., Quinn, P. K., Bates, T. S., Meagher, J. F., Fehsenfeld, F. C., and Ravishankara, A. R.: Nighttime removal of NO_x in the summer marine boundary layer, Geophys. Res. Lett., 31, L07108, doi:10.1029/2004GL019412, 2004.

Buhr, M.: Measurement of NO_2 in ambient air using a solid-state photolytic converter, in: Symposium on Air Quality Measurement Methods and Technology 2004, 20–22 April 2004, 165–171, Cary, NC, USA, 2004.

Buhr, M.: Solid-State Light Source Photolytic Nitrogen Dioxide Converter, US 7238328 B2, 3 July 2007.

ACPD
15, 28699–28747, 2015

Cantrell, C. A., Shetter, R. E., Calvert, J. G., Eisele, F. L., Williams, E., Baumann, K., Brune, W. H., Stevens, P. S., and Mather, J. H.: Peroxy radicals from photostationary state deviations and steady state calculations during the Tropospheric OH Photochemistry Experiment at Idaho Hill, Colorado, 1993, J. Geophys. Res., 102, 6369, doi:10.1029/96JD01703, 1997.

Cantrell, C. A., Mauldin, L., Zondlo, M., Eisele, F. L., Kosciuch, E., Shetter, R. E., Lefer, B., Hall, S., Campos, T. L., Ridley, B., Walega, J. G., Fried, A., Wert, B., Flocke, F. M., Weinheimer, A. J., Hannigan, J., Coffey, M., Atlas, E., Stephens, S., Heikes, B. G., Snow, J., Blake, D. R., Blake, N., Katzenstein, A., Lopez, J., Browell, E. V., Dibb, J. E., Scheuer, E., Seid, G., and Talbot, R. W.: Steady state free radical budgets and ozone photochemistry during TOPSE, J. Geophys. Res., 108, 8361, doi:10.1029/2002JD002198, 2003.

Carbajo, P. G. and Orr-Ewing, A. J.: NO_2 quantum yields from ultraviolet photodissociation of methyl and isopropyl nitrate., Phys. Chem. Chem. Phys., 12, 6084–6091, doi:10.1039/c001425g, 2010.

Carslaw, D. C.: Evidence of an increasing NO_2/ NO_x emissions ratio from road traffic emissions, Atmos. Environ., 39, 4793–4802, doi:10.1016/j.atmosenv.2005.06.023, 2005.

Clyne, M. A. A., Thrush, B. A., and Wayne, R. P.: Kinetics of the chemiluminescent reaction between nitric oxide and ozone, Trans. Faraday Soc., 60, 359–370, doi:10.1039/TF9646000359, 1964.

Crutzen, P. J.: The role of NO and NO_2 in the chemistry of the troposphere and stratosphere, Annu. Rev. Earth Panetary Sci., 7, 443–472, doi:10.1146/annurev.ea.07.050179.002303, 1979.

Dalsøren, S. B. and Isaksen, I. S. A.: CTM study of changes in tropospheric hydroxyl distribution 1990–2001 and its impact on methane, Geophys. Res. Lett., 33, L23811, doi:10.1029/2006GL027295, 2006.

Dari-Salisburgo, C., Di Carlo, P., Giammaria, F., Kajii, Y., and D'Altorio, A.: Laser induced fluorescence instrument for NO_2 measurements: observations at a central Italy background site, Atmos. Environ., 43, 970–977, doi:10.1016/j.atmosenv.2008.10.037, 2009.

Day, D. A., Wooldridge, P. J., Dillon, M. B., Thornton, J. A., and Cohen, R. C.: A thermal dissociation laser-induced fluorescence instrument for in situ detection of NO_2, peroxy nitrates, alkyl nitrates, and HNO_3, J. Geophys. Res., 107, ACH 4-1–ACH 4-14, doi:10.1029/2001JD000779, 2002.

ACPD
15, 28699–28747, 2015

Dentener, F. J. and Crutzen, P. J.: Reaction of N_2O_5 on tropospheric aerosols: impact on the global distributions of NO_x, O_3, and OH, J. Geophys. Res., 94, 7149–7163, doi:10.1029/92JD02979, 1993.

Di Carlo, P., Aruffo, E., Busilacchio, M., Giammaria, F., Dari-Salisburgo, C., Biancofiore, F., Visconti, G., Lee, J., Moller, S., Reeves, C. E., Bauguitte, S., Forster, G., Jones, R. L., and Ouyang, B.: Aircraft based four-channel thermal dissociation laser induced fluorescence instrument for simultaneous measurements of NO_2, total peroxy nitrate, total alkyl nitrate, and HNO_3, Atmos. Meas. Tech., 6, 971–980, doi:10.5194/amt-6-971-2013, 2013.

Drummond, J. W., Volz, A., and Ehhalt, D. H.: An optimized chemiluminescence detector for tropospheric NO measurements, J. Atmos. Chem., 2, 287–306, doi:10.1007/BF00051078, 1985.

Dunlea, E. J., Herndon, S. C., Nelson, D. D., Volkamer, R. M., San Martini, F., Sheehy, P. M., Zahniser, M. S., Shorter, J. H., Wormhoudt, J. C., Lamb, B. K., Allwine, E. J., Gaffney, J. S., Marley, N. A., Grutter, M., Marquez, C., Blanco, S., Cardenas, B., Retama, A., Ramos Villegas, C. R., Kolb, C. E., Molina, L. T., and Molina, M. J.: Evaluation of nitrogen dioxide chemiluminescence monitors in a polluted urban environment, Atmos. Chem. Phys., 7, 2691–2704, doi:10.5194/acp-7-2691-2007, 2007.

Fehsenfeld, F. C., Dickerson, R. R., Hobler, G., Luke, W. T., Nunnermacker, L. J., Roberts, J. M., Curran, C. M., Eubank, C. S., Fahey, D. W., Mindplay, P. C., and Pickering, K. E.: A ground-based intercomparison of NO, NO_x, and NO_y measurement techniques, J. Geophys. Res., 92, 710–722, doi:10.1029/JD092iD12p14710, 1987.

Fehsenfeld, F. C., Drummond, J. W., Roychowdhury, U. K., Galvin, P. J., Williams, E. J., Burr, M. P., Parrish, D. D., Hobler, G., Langford, A. O., Calvert, J. G., Ridley, B. A., Heikes, B. G., Kok, G. L., Shetier, J. D., Walega, J. G., Elsworth, C. M., and Mohnen, V. A.: Intercomparison of NO_2 measurement techniques, J. Geophys. Res., 95, 3579–3597, doi:10.1029/JD095iD04p03579, 1990.

Fischer, G. and Nwankwoala, A. U.: A spectroscopic study of the thermal decomposition of peroxyacetyl nitrate (PAN), Atmos. Environ., 29, 3277–3280, doi:10.1016/1352-2310(95)00252-T, 1995.

Fontijn, A., Sabadell, A. J., and Ronco, R. J.: Homogeneous chemiluminescent measurement of nitric oxide with ozone. Implications for continuous selective monitoring of gaseous air pollutants, Anal. Chem., 42, 575–579, doi:10.1021/ac60288a034, 1970.

ACPD
15, 28699–28747, 2015

Frey, M. M., Brough, N., France, J. L., Anderson, P. S., Traulle, O., King, M. D., Jones, A. E., Wolff, E. W., and Savarino, J.: The diurnal variability of atmospheric nitrogen oxides (NO and NO_2) above the Antarctic Plateau driven by atmospheric stability and snow emissions, Atmos. Chem. Phys., 13, 3045–3062, doi:10.5194/acp-13-3045-2013, 2013.

Frey, M. M., Roscoe, H. K., Kukui, A., Savarino, J., France, J. L., King, M. D., Legrand, M., and Preunkert, S.: Atmospheric nitrogen oxides (NO and NO_2) at Dome C, East Antarctica, during the OPALE campaign, Atmos. Chem. Phys., 15, 7859–7875, doi:10.5194/acp-15-7859-2015, 2015.

Gardner, E. P., Sperry, P. D., and Calvert, J. G.: Primary quantum yields of NO_2 photodissociation, J. Geophys. Res., 92, 6642–6652, doi:10.1029/JD092iD06p06642, 1987.

Hollaway, M. J., Arnold, S. R., Challinor, A. J., and Emberson, L. D.: Intercontinental transboundary contributions to ozone-induced crop yield losses in the Northern Hemisphere, Biogeosciences, 9, 271–292, doi:10.5194/bg-9-271-2012, 2012.

Hosaynali Beygi, Z., Fischer, H., Harder, H. D., Martinez, M., Sander, R., Williams, J., Brookes, D. M., Monks, P. S., and Lelieveld, J.: Oxidation photochemistry in the Southern Atlantic boundary layer: unexpected deviations of photochemical steady state, Atmos. Chem. Phys., 11, 8497–8513, doi:10.5194/acp-11-8497-2011, 2011.

Huntrieser, H., Schlager, H., Roiger, A., Lichtenstern, M., Schumann, U., Kurz, C., Brunner, D., Schwierz, C., Richter, A., and Stohl, A.: Lightning-produced NO_x over Brazil during TROCCINOX: airborne measurements in tropical and subtropical thunderstorms and the importance of mesoscale convective systems, Atmos. Chem. Phys., 7, 2987–3013, doi:10.5194/acp-7-2987-2007, 2007.

Kelly, T. J., Stedman, D. H., Ritter, J. A., and Harvey, R. B.: Measurements of oxides of nitrogen and nitric acid in clean air, J. Geophys. Res., 85, 7417–7425, doi:10.1029/JC085iC12p07417, 1980.

Kleindienst, T. E.: Recent developments in the chemistry and biology of peroxyacetyl nitrate, Res. Chem. Intermed., 20, 335–384, doi:10.1163/156856794X00379, 1994.

Kley, D., Drummond, J. W., McFarland, M., and Liu, S. C.: Tropospheric profiles of NO_x, J. Geophys. Res., 86, 3153–3161, doi:10.1029/JC086iC04p03153, 1981.

Koepke, P., Garhammer, M., Hess, M., and Roeth, E.-P.: NO_2 photolysis frequencies in street canyons, Atmos. Chem. Phys., 10, 7457–7466, doi:10.5194/acp-10-7457-2010, 2010.

ACPD
15, 28699–28747, 2015

Lee, J. D., Moller, S. J., Read, K. A., Lewis, A. C., Mendes, L., and Carpenter, L. J.: Year-round measurements of nitrogen oxides and ozone in the tropical North Atlantic marine boundary layer, J. Geophys. Res., 114, D21302, doi:10.1029/2009JD011878, 2009.

Leighton, P. A.: Photochemistry of Air Pollution, Academic Press, University of Michigan, Ann Arbor, Michigan, USA, 1961.

Lelieveld, J., Dentener, F. J., Peters, W., and Krol, M. C.: On the role of hydroxyl radicals in the self-cleansing capacity of the troposphere, Atmos. Chem. Phys., 4, 2337–2344, doi:10.5194/acp-4-2337-2004, 2004.

Levy II, H.: Photochemistry of the lower troposphere, Planet. Space Sci., 20, 919–935, doi:10.1016/0032-0633(72)90177-8, 1972.

Matsumoto, J. and Kajii, Y.: Improved analyzer for nitrogen dioxide by laser-induced fluorescence technique, Atmos. Environ., 37, 4847–4851, doi:10.1016/j.atmosenv.2003.08.023, 2003.

Matsumoto, J., Hirokawa, J., Akimoto, H., and Kajii, Y.: Direct measurement of NO_2 in the marine atmosphere by laser-induced fluorescence technique, Atmos. Environ., 35, 2803–2814, doi:10.1016/S1352-2310(01)00078-4, 2001.

Mauzerall, D. L., Sultan, B., Kim, N., and Bradford, D. F.: NO emissions from large point sources: variability in ozone production, resulting health damages and economic costs, Atmos. Environ., 39, 2851–2866, doi:10.1016/j.atmosenv.2004.12.041, 2005.

Mazely, T. L., Friedl, R. R., and Sander, S. P.: Production of NO_2 from photolysis of peroxyacetyl nitrate, J. Phys. Chem., 99, 8162–8169, doi:10.1021/j100020a044, 1995.

Meyrahn, H., Helas, G., and Warneck, P.: Gas chromatographic determination of peroxyacetyl nitrate: two convenient calibration techniques, J. Atmos. Chem., 5, 405–415, doi:10.1007/BF00113903, 1987.

Mills, G. P., Sturges, W. T., Salmon, R. A., Bauguitte, S. J.-B., Read, K. A., and Bandy, B. J.: Seasonal variation of peroxyacetylnitrate (PAN) in coastal Antarctica measured with a new instrument for the detection of sub-part per trillion mixing ratios of PAN, Atmos. Chem. Phys., 7, 4589–4599, doi:10.5194/acp-7-4589-2007, 2007.

Moore, R. M. and Blough, N. V.: A marine source of methyl nitrate, Geophys. Res. Lett., 29, 27-1–27-4, doi:10.1029/2002GL014989, 2002.

Osthoff, H. D., Brown, S. S., Ryerson, T. B., Fortin, T. J., Lerner, B. M., Williams, E. J., Pettersson, A., Baynard, T., Dubé, W. P., Ciciora, S. J., and Ravishankara, A. R.: Measurement of

ACPD
15, 28699–28747, 2015

atmospheric NO_2 by pulsed cavity ring-down spectroscopy, J. Geophys. Res., 111, D12305, doi:10.1029/2005JD006942, 2006.
Pandey, S. K., Kim, K. H., Chung, S. Y., Cho, S. J., Kim, M. Y., and Shon, Z. H.: Long-term study of NO_x behavior at urban roadside and background locations in Seoul, Korea, Atmos. Environ., 42, 607–622, doi:10.1016/j.atmosenv.2007.10.015, 2008.
Penkett, S., Gilge, S., Plass-Duelmer, C., Galbally, I., Brough, N., Bottenheim, J. W., Flocke, F. M., Gerwig, H., Lee, J. D., Milton, M., Roher, F., Ryerson, T. B., Steinbacher, M., Torseth, K., Wielgosz, R., Suda, K., Akimoto, H., and Tarasova, O.: A WMO/GAW Expert Workshop on Global Long-term Measurements of Nitrogen Oxides and Recommendations for GAW Nitrogen Oxides Network, Hohenpeissenberg, Germany, 8–9 October 2009, WMO TD No. 1570, 45 pp., February 2011.
Peterson, C. and Honrath, R. E.: NO_x and NO_y over the northwestern North Atlantic: measurements and measurement accuracy, J. Geophys. Res. Atmos., 104, 11695–11707, doi:10.1029/1998JD100088, 1999.
Pollack, I. B., Lerner, B. M., and Ryerson, T. B.: Evaluation of ultraviolet light-emitting diodes for detection of atmospheric NO_2 by photolysis – chemiluminescence, J. Atmos. Chem., 65, 111–125, doi:10.1007/s10874-011-9184-3, 2011.
Ridley, B. A., Carroll, M. A., Torres, A. L., Condon, E. P., Sachse, G. W., Hill, G. F., and Gregory, G. L.: An intercomparison of results from ferrous sulphate and photolytic converter techniques for measurements of NO_x made during the NASA GTE/CITE 1 aircraft program, J. Geophys. Res., 93, 15803–15811, doi:10.1029/JD093iD12p15803, 1988.
Riemer, N., Vogel, H., Vogel, B., Schell, B., Ackermann, I., Kessler, C., and Hass, H.: Impact of the heterogeneous hydrolysis of N_2O_5 on chemistry and nitrate aerosol formation in the lower troposphere under photosmog conditions, J. Geophys. Res., 108, 1–21, doi:10.1029/2002JD002436, 2003.
Roumelis, N. and Glavas, S.: Thermal decomposition of peroxyacetyl nitrate in the presence of O_2, NO_2 and NO, Monatsh. Chem., 123, 63–72, doi:10.1007/BF01045298, 1992.
Ryerson, T. B., Williams, E. J., and Fehsenfeld, F. C.: An efficient photolysis system for fast-response NO_2 measurements, J. Geophys. Res., 105, 26447–26461, doi:10.1029/2000JD900389, 2000.
Sadanaga, Y., Fukumori, Y., Kobashi, T., Nagata, M., Takenaka, N., and Bandow, H.: Development of a selective light-emitting diode photolytic NO_2 converter for continuously measuring NO_2 in the atmosphere, Anal. Chem., 82, 9234–9239, doi:10.1021/ac101703z, 2010.

ACPD
15, 28699–28747, 2015

Sander, S. P., Golden, D. M., Kurylo, M. J., Moorgat, G. K., Keller-Rudek, H., Wine, P. H., Ravishankara, A. R., Kolb, C. E., Molina, M. J., Finlayson-Pitts, B. J., Huie, R. E., and Orkin, V. L.: Chemical Kinetics and Photochemical Data for Use in Atmospheric Studies, Evaluation No. 17, JPL Publication 10-6, Jet Propulsion Laboratory, Pasadena, USA, available at: http://jpldataeval.jpl.nasa.gov (last access: 22 October 2015), 2011.

Schott: Schott UG5 UV-passing filter, datasheet, available at: http://www.uqgoptics.com/materials_filters_schott_uvTransmitting_UG5.aspx (last access: 25 July 2014), 1997.

Sherwen, T., Evans, M. J., Carpenter, L. J., Andrews, S. J., Lidster, R. T., Dix, B., Koenig, T. K., Volkamer, R., Saiz-Lopez, A., Prados-Roman, C., Mahajan, A. S., and Ordóñez, C.: Iodine's impact on tropospheric oxidants: a global model study in GEOS-Chem, Atmos. Chem. Phys. Discuss., 15, 20957–21023, doi:10.5194/acpd-15-20957-2015, 2015.

Skalska, K., Miller, J. S., and Ledakowicz, S.: Trends in NO_x abatement: a review., Sci. Total Environ., 408, 3976–3989, doi:10.1016/j.scitotenv.2010.06.001, 2010.

Stieb, D. M., Judek, S., and Burnett, R. T.: Meta-analysis of time-series studies of air pollution and mortality: effects of gases and particles and the influence of cause of death, age, and season, J. Air Waste Manag. Assoc., 52, 470–484, doi:10.1080/10473289.2002.10470794, 2002.

Talukdar, R. K., Burkholder, J. B., Hunter, M., Gilles, M. K., Roberts, J. M., and Ravishankara, A. R.: Atmospheric fate of several alkyl nitrates Part 2 UV absorption cross-sections and photodissociation quantum yields, J. Chem. Soc. Faraday Trans., 93, 2797–2805, doi:10.1039/A701781B, 1997.

Thornton, J. A., Wooldridge, P. J., and Cohen, R. C.: Atmospheric NO_2: in situ laser-induced fluorescence detection at parts per trillion mixing ratios, Anal. Chem., 72, 528–39, 2000.

Tuazon, E. C., Carter, W. P. L., and Atkinson, R.: Thermal decomposition of peroxyacetyl nitrate and reactions of acetyl peroxy radicals with NO and NO_2 over the temperature range 283–313 K, J. Phys. Chem., 95, 2434–2437, doi:10.1021/j100159a059, 1991.

Tuzson, B., Zeyer, K., Steinbacher, M., McManus, J. B., Nelson, D. D., Zahniser, M. S., and Emmenegger, L.: Selective measurements of NO, NO_2 and NO_y in the free troposphere using quantum cascade laser spectroscopy, Atmos. Meas. Tech., 6, 927–936, doi:10.5194/amt-6-927-2013, 2013.

Val Martin, M., Honrath, R. E., Owen, R. C., and Li, Q. B.: Seasonal variation of nitrogen oxides in the central North Atlantic lower free troposphere, J. Geophys. Res., 113, D17307, doi:10.1029/2007JD009688, 2008.

ACPD
15, 28699–28747, 2015

Villena, G., Bejan, I., Kurtenbach, R., Wiesen, P., and Kleffmann, J.: Interferences of commercial NO_2 instruments in the urban atmosphere and in a smog chamber, Atmos. Meas. Tech., 5, 149–159, doi:10.5194/amt-5-149-2012, 2012.

Wang, W.-C., Liang, X.-Z., Dudek, M. P., Pollard, D., and Thompson, S. L.: Atmospheric ozone as a climate gas, Atmos. Res., 37, 247–256, doi:10.1016/0169-8095(94)00080-W, 1995.

Warneck, P. and Zerbach, T.: Synthesis of peroxyacetyl nitrate in air by acetone photolysis, Environ. Sci. Technol., 26, 74–79, doi:10.1021/es00025a005, 1992.

Whalley, L. K., Lewis, A. C., McQuaid, J. B., Purvis, R. M., Lee, J. D., Stemmler, K., Zellweger, C., and Ridgeon, P.: Two high-speed, portable GC systems designed for the measurement of non-methane hydrocarbons and PAN: results from the Jungfraujoch High Altitude Observatory, J. Environ. Monit., 6, 234–41, doi:10.1039/b310022g, 2004.

Zellweger, C., Ammann, M., Buchmann, B., Hofer, P., Lugauer, M., Streit, N., Weingartner, E., and Baltensperger, U.: Summertime NO_y speciation at the Jungfraujoch, 3580 m above sea level, Switzerland, J. Geophys. Res., 105, 6655–6667, doi:10.1029/1999JD901126, 2000.

Zhang, L., Wiebe, A., Vet, R., Mihele, C., O'Brien, J. M., Iqbal, S., and Liang, Z.: Measurements of reactive oxidized nitrogen at eight Canadian rural sites, Atmos. Environ., 42, 8065–8078, doi:10.1016/j.atmosenv.2008.06.034, 2008.

ACPD
15, 28699–28747, 2015

Table 1. Comparison of the NO_2 signal observed from measurement of three zero air sources. (Eco Physics AG PAG 003, BOC Specialty Gasses BTCA 178, and Sofnofil/Carbon/13× molecular sieve filters) by LIF. The average of ten 1 min averages is shown in raw PMT counts per second as well as the standard deviation of those averages.

	PAG 003	BTCA 178	Sofnofil/Carbon
Signal (cps)	88.10	88.66	83.95
Standard Deviation	1.64	1.56	1.81

ACPD
15, 28699–28747, 2015

Table 2. Effect of varying the residence time of PAN (1.0 ppb) within a 2.7 m PFA inlet on measured NO_2 concentrations.

	Inlet residence time (s^{-1})			
	0.84	1.05	1.40	2.10
NO_2 (ppt)	60.2	61.3	60.6	61.5
NO_2 (%)	5.4	5.4	5.2	5.3

ACPD
15, 28699–28747, 2015

Table 3. Peak surface temperature and current drawn by BLC lamps in a bench test at 20.0 °C showing converter efficiency, current, and surface temperature.

Lamp No.	Converter efficiency (%) ±1	BLC Lamp Surface Temperature (°C) ±0.05	Current Draw (A) ±0.0005
1	41	79.8	0.969
2		75.3	0.953
3	35	77.6	0.933
4		74.0	0.931
5	22	76.2	0.916
6		56.4	0.567

ACPD
15, 28699–28747, 2015

Table 4. The average percentage conversion of PAN to NO_2 measured, and normalized to the converter efficiency of each BLC.

	Converter efficiency (%) ±1		
	42	33	22
Measured %	10.8	15.9	19.6
Normalized %	4.4	5.2	4.3

ACPD
15, 28699–28747, 2015

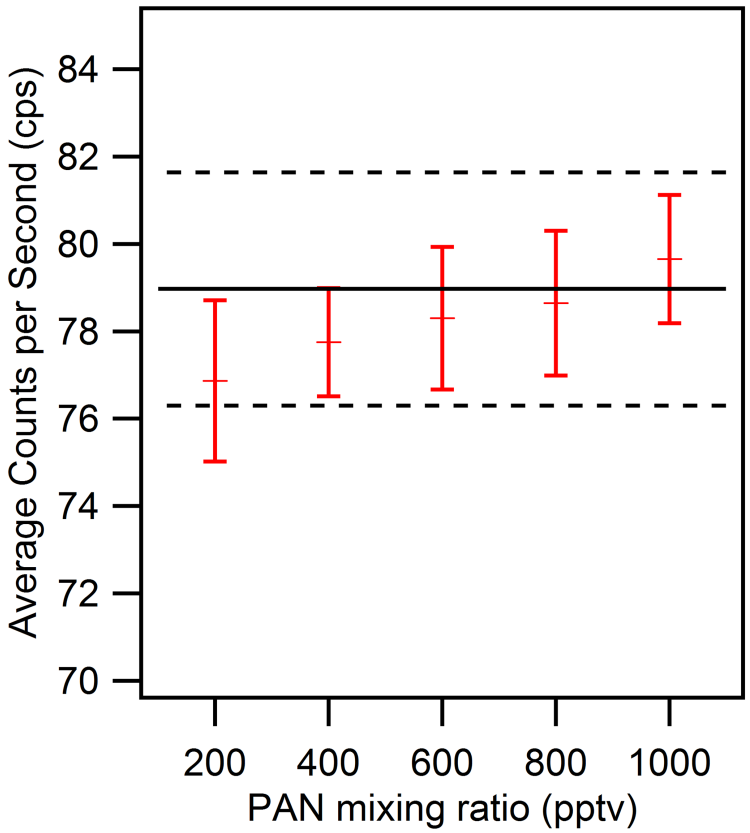

Figure 1. The average raw counts per second recorded by a LIF instrument when sampling various mixing ratios of PAN (in red) and zero air (black). The variance of the zero air signal is also shown (dashed black). The average signal while sampling PAN falls within the noise of the zero signal.

ACPD
15, 28699–28747, 2015

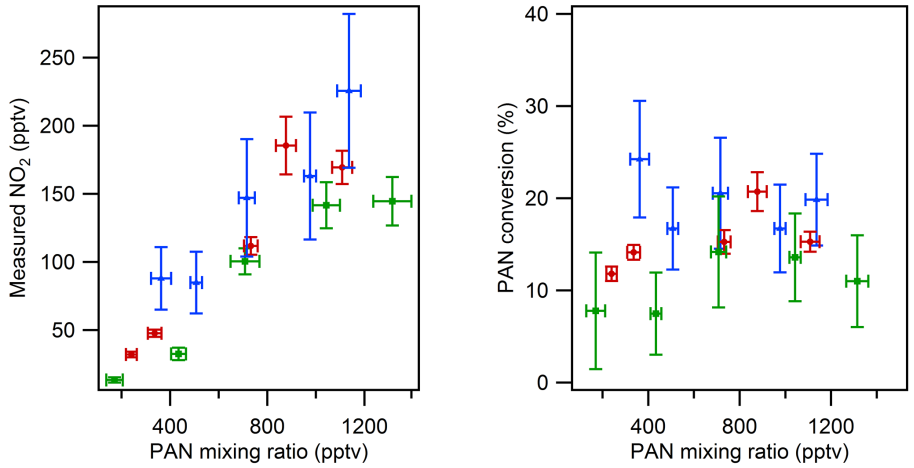

Figure 2. The measured absolute NO_2 signal (left panel) of the supplied PAN mixing ratio, and as a percentage (right panel), for three BLC units operating in constant mode. Green = 41 % CE, Red = 35 % CE, Blue = 22 % CE.

ACPD
15, 28699–28747, 2015

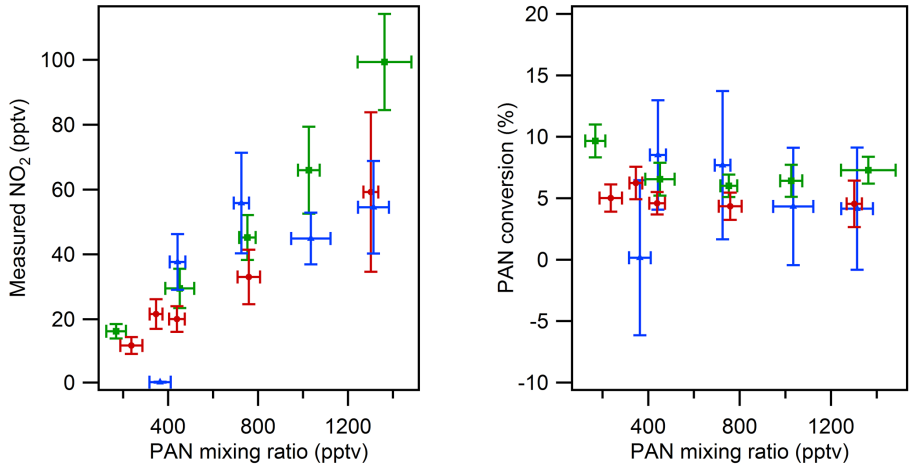

Figure 3. The measured absolute NO_2 signal as a function of the supplied PAN mixing ratio (left panel), and as a percentage (right panel), for three BLC units operating in switching mode. Green = 41 % CE, Red = 35 % CE, Blue = 22 % CE.

ACPD
15, 28699–28747, 2015

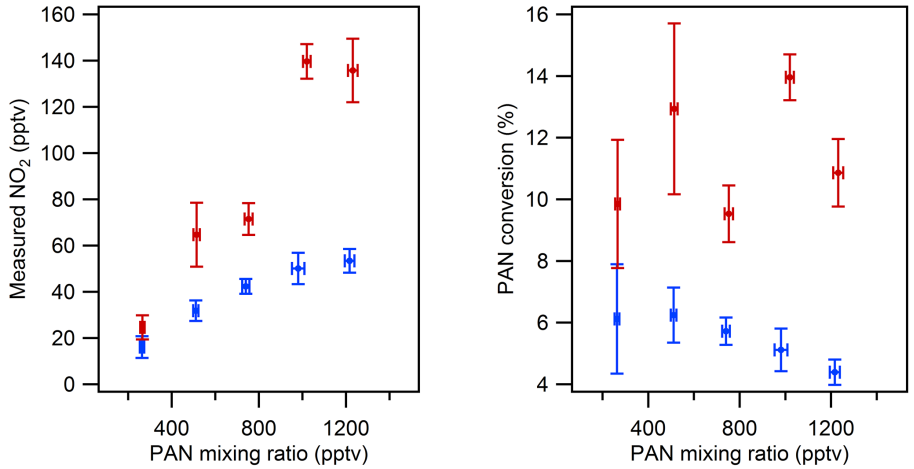

Figure 4. The measured NO_2 signal as a function of the supplied PAN mixing ratio (left panel), and as a percentage (right panel), for the cooled (blue) and uncooled (red) high powered BLC.

ACPD
15, 28699–28747, 2015

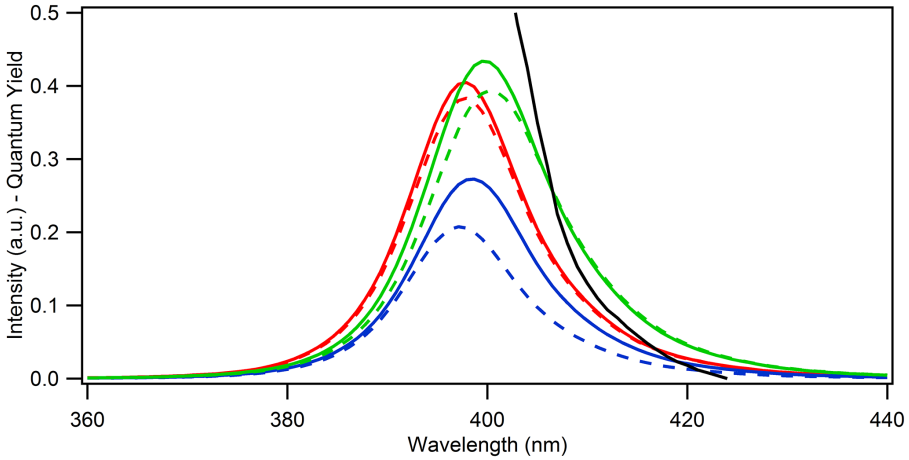

Figure 5. Shown is the spectral output vs. wavelength of two new, previously unused BLC lamps No. 1 (solid) and 2 (dashed) in green, two used lamps No. 3 (solid) and 4 (dashed) in red; still within acceptable conversion efficiency, and two which fall below acceptable limits No. 5 (solid) and 6 (dashed) in blue. The NO_2 quantum yield is shown in black.

ACPD
15, 28699–28747, 2015

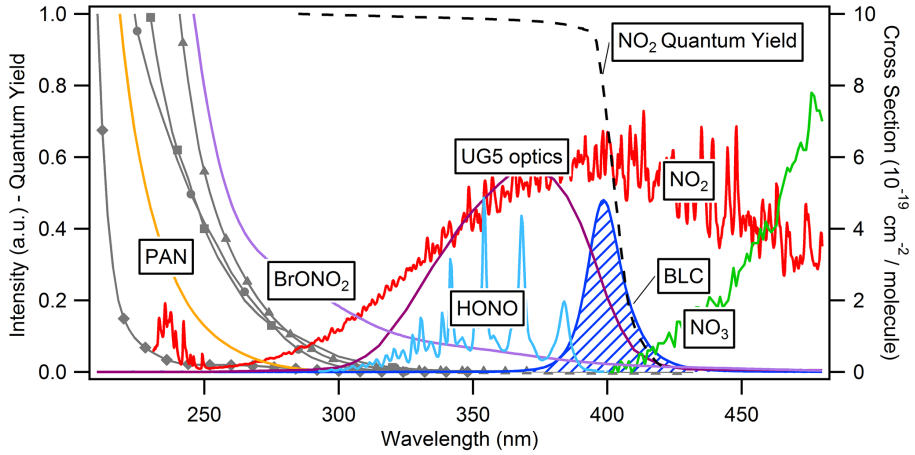

Figure 6. Absorption cross section (red) and quantum yield (dashed black) of NO_2, presented with the spectral output of UG5 optical filtering (purple) and an average of the six BLC lamps used in this study output (dark blue). Shown are interfering species; NO_3 radicals (green), HONO (light blue), $BrONO_2$ (lilac) which are overlapped significantly by the UG5 optics – completely in the case of HONO, whilst much less overlap is exhibited by the UV-LEDs of the BLC. Also shown is PAN (gold), which clearly is not overlapped by either UG5 or BLC light sources. Additional non-interfering species; $ClONO_2$ (triangles), N_2O_5 (squares), HO_2NO_2 (circles), HNO_3 (diamonds) shown for reference.

ACPD
15, 28699–28747, 2015

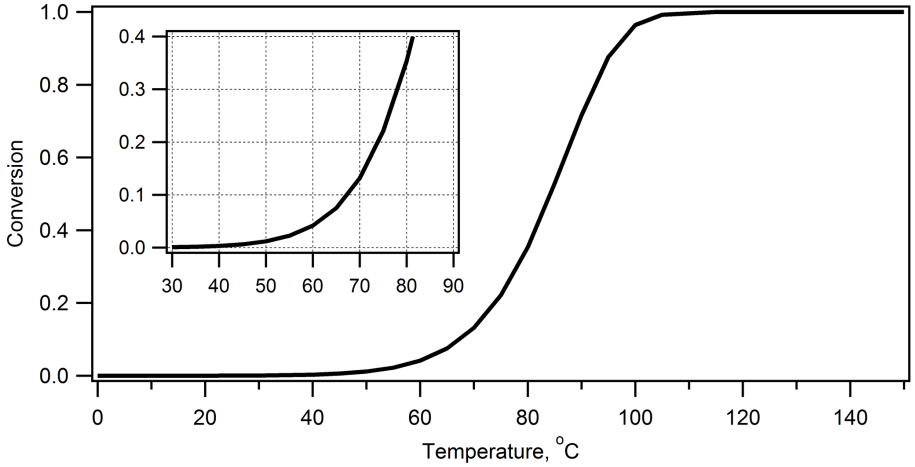

Figure 7. Model of thermal decomposition of PAN to NO_2 with a residence time of 0.96 s at temperatures between 0 to 150 °C. Inset is detail of 30 to 90 °C.

ACPD
15, 28699–28747, 2015

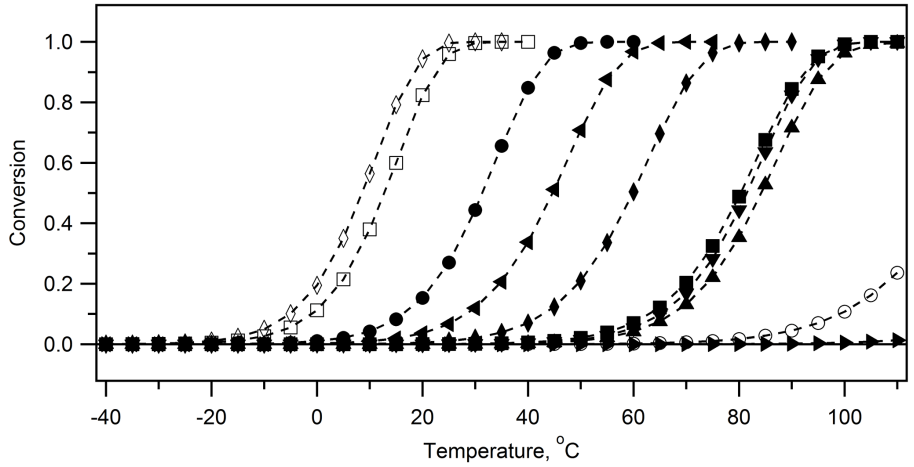

Figure 8. Thermal decomposition profiles of $IONO_2$ ♦; $BrONO_2$ ○; $ClONO_2$ ►; HO_2NO_2 •; N_2O_5 ◄; $C_2H_5O_2NO_2$ ⋄; $CH_3C(O)CH_2O_2NO_2$ □; MPAN ■; PAN ▲; PPN ▼. Calculated from IUPAC recommended kinetic data using FACSIMILE software based on 1 s residence time. Note $CH_3O_2NO_2$ is not shown but has the same profile as HO_2NO_2.

ACPD
15, 28699–28747, 2015

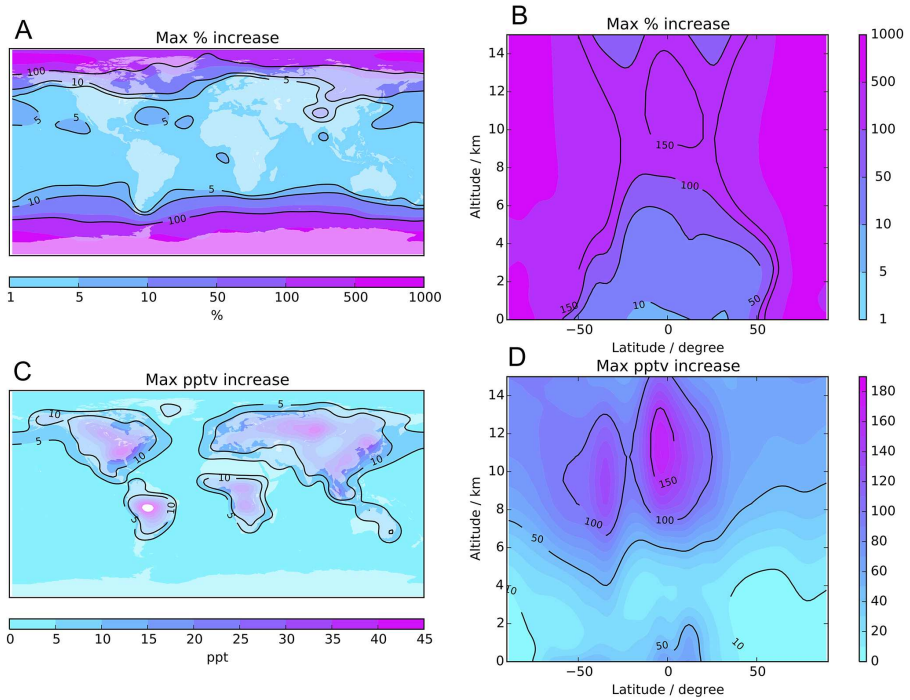

Figure 9. GEOS-Chem model showing the monthly maximum percentage over-reporting of NO_2 **(a)** zonally and **(b)** by altitude in any month of a 1 year simulation. Panels **(c)** and **(d)** show the same in absolute pptv values. Note; the area over the Amazon in plot **(c)** is over the maximum range of the colour scale. Surface values are the maximum over-reporting in any month, zonal values are the maximum over reporting in any month and in any of the longitudinal grid boxes.

ACPD
15, 28699–28747, 2015

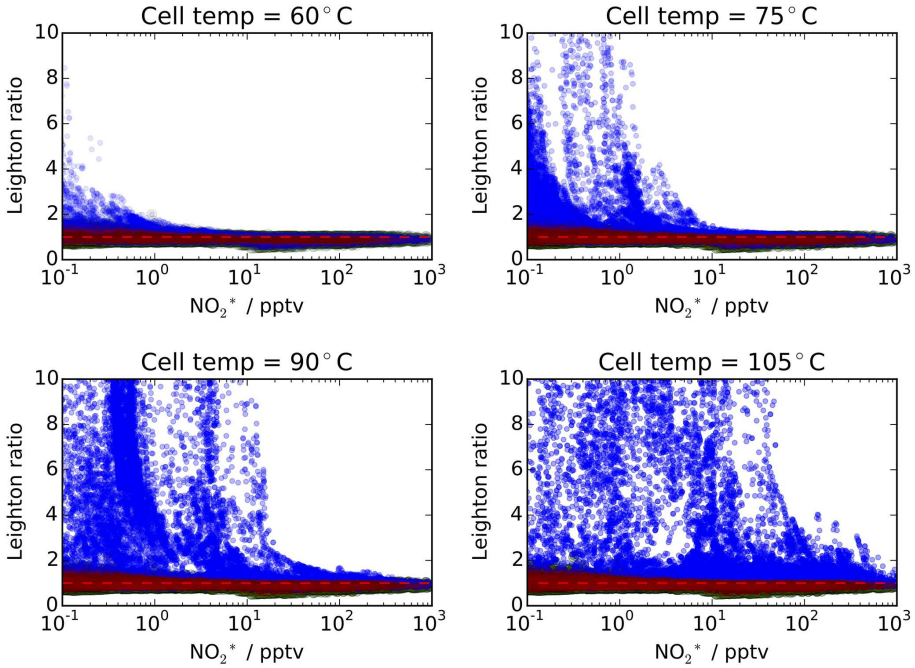

Figure 10. Leighton ratio calculated for each model grid-box for each daylight hour for March by the model as a function of the grid box NO_2 concentration. The instrument interference is characterized by a numerical solution of Eq. (5) with $\tau = 0.42$ s and a residence time of 1 s. Red shows the values calculated without the interference on the NO_2 concentration and the blue indicated the values calculated with the interference. The interferences are calculated for different lamp temperatures, 65 to 105 °C.

ACPD
15, 28699–28747, 2015